PERGAMON

International Journal of Heat and Mass Transfer 44 (2001) 4059–4073

International Journal of HEAT and MASS TRANSFER

www.elsevier.com/locate/ijhmt

A statistical model of wave scattering from random rough surfaces

Kakuen Tang [a], Richard O. Buckius [b,*]

[a] *Boeing Satellite Systems, El Segundo, CA, USA*

[b] *Department of Mechanical and Industrial Engineering, University of Illinois at Urbana-Champaign, 140 Mech. Eng. Building, MC-244, 1206 West Green Street, Urbana, IL 61801, USA*

Received 23 June 1999; received in revised form 2 January 2001

Abstract

A statistical model based on the geometric optics approximation for predicting wave scattering from random rough surfaces is developed. This model uses statistical concepts, rather than bundle tracing employed in the geometric optics approximation. This model includes first-, second- and higher-order scatterings. Shadowing effects are included, and the model can be expressed in a closed form. For one-dimensional random rough surfaces, the statistical model is quantified by comparisons with the exact electromagnetic theory calculations, and the results are in good agreement for surfaces with a surface slope less than unity. For two-dimensional random rough surfaces, the approximate results are compared with the existing experimental findings and electromagnetic theory calculations. The statistical method is a computationally inexpensive wave scattering approach for surfaces with a surface slope less than 0.5, and the method can approximate the magnitude and the trend for surfaces with a surface slope greater than 0.5.

1. Introduction

Scattering problems have been extensively studied both analytically and experimentally. The analytical approaches have considered both rigorous electromagnetic theory methods and approximate models. Rigorous electromagnetic theory provides exact solutions to surface reflection problems without any restriction on incident angles, incident wavelengths, optical constants of surface materials, correlation length and surface roughness. This approach involves multiple coupled integral equations, which can only be solved analytically for a few limited cases. Thus, numerical schemes are typically required. In addition, due to computational limitations, the ability to predict such reflection distributions from general random rough surfaces through electromagnetic theory has only recently been developed, and results are available only for one-dimensional surfaces (two-dimensional electromagnetic fields) in general [1–14], and for two-dimensional surfaces (three-dimensional electromagnetic fields) in limited cases [15–22].

Rigorous electromagnetic theory analysis of surface reflection is very computationally intensive. This is especially true for random rough surfaces since a statistically accurate result has to be averaged over numerous surface realizations. Thus, various surface scattering approximations have been developed to circumvent these difficulties. Two often-used approximations are the specular (Fresnel) [23] and diffuse (Lambertian) [24] models. The specular model assumes that energy is reflected in the solid angle region around the specular angle ($\theta_s = \theta_o$), while in the diffuse model, energy is assumed to be equally distributed in all directions. The Kirchhoff approximation [25] is used to predict the reflection distribution between the specular and diffuse reflection. At every point on the surface, the scattered magnetic and electric fields are approximated by the field that would exist on a plane tangent to the surface at this point. The Kirchhoff approximation has been applied to both one-dimensional and two-dimensional random

* Corresponding author. Tel.: +1-217-333-1079; fax: 1-217-244-6534.

E-mail address: buckius@uiuc.edu (R.O. Buckius).

0017-9310/01/$ - see front matter
PII: S0017-9310(01)00050-3

Nomenclature

A_o	incident area
A_p	projected area
A_s	reflecting area
C	set of normals
E	criterion ratio
e	fraction of incoming energy
F	Fresnel reflection coefficients
f	probability density function
g	conditional probability
I	intensity
n	surface refractive index
$\mathbf{r}$	position vectors
S	shadowing function
t	transfer function
x, y, z	surface coordinates
z_x, z_y	partial derivatives

Greek symbols

α_o, α_s	angles between beam and normal vectors
Φ	radiant power flow
ϕ	Azimuthal angle
λ	wavelength
θ	polar angle
ρ'', ρ'	bi-directional reflectivity; directional reflectivity
σ	roughness
σ_{rms}	rms surface slope
τ	surface correlation length
τ'', τ'	bi-directional transmissivity; directional transmissivity
κ	absorption index
Ω	scattering direction, solid angle
ζ	surface profile
ζ_x, ζ_y	surface derivatives

Subscripts

1	first-order scattering
2	second-order scattering
3	third-order scattering
a	approximate solution
cr	critical value
d	directional criterion, directly reflected
dd	directional diffuse
e	exact solution
H	higher-order scattering
m	mean value
o	incident
s	scattered
sp	specular
t	transmission
x, y, z	coordinates

Superscripts

$'$	hemispherical
$''$	bi-directional

rough surfaces and domains of validity have been constructed [26–29]. It is commonly believed that the Kirchhoff approximation yields an accurate solution when the surface geometric parameters are comparable with the incident wavelength and the ratio of surface roughness to correlation length is less than 0.3.

The geometric optics approximation to electromagnetic theory provides a multiple scattering solution for surface reflection. In this approximation the energy incident on a rough surface is traced through multiple interactions with the surface until it leaves the surface, and Fresnel reflection is applied to each local point of intersection. For a rough surface, the number of interactions typically increases with surface slope. For a plane surface, the geometric optics approximation reduces to the Fresnel reflection since all the energy is reflected in the solid angle region around the specular angle. Tang et al. [30,31] have shown that the geometric optics model can provide accurate solution for one-dimensional random rough surfaces with $\sigma/\tau < 4.0$ and for two-dimensional surfaces with $\sigma/\tau < 1.0$.

Probability and statistical concepts have often been applied to wave scattering phenomena. In general, these statistical models provide a closed form solution, and the numerical requirements are less demanding than other methods. The basic elements of statistical models are incoming and outgoing shadowing functions. The incoming shadowing function is the probability that a surface point does not lie in a shadowed region for a specified incident angle, and this probability is equal to the outgoing shadowing function which is the probability that an energy bundle reflected at a specified angle will not re-strike the surface. Various geometrical shadowing functions [32–36] have been developed for Gaussian random rough surfaces and then employed in reflection models. Wagner [33] developed shadowing functions in which the correlation between surface height and surface slope at one point is neglected. The correlation of surface heights and surface slopes between points is also neglected. This function is a closed form solution involving error functions, correlation length, surface deviation and incident angle. Lynch and Wagner [37] adopted this function and developed a light reflection model based on the ray nature of light, and this model includes first and second-order scatterings. The shadowing function is the basic component of this reflection model. The solution involved numerous algebraic equations. In addition, based on the input parameters, different equations are used to generate the reflection distributions. No comparison has been made

for quantifying the model and the domain of validity is unknown.

Smith [32] developed a similar uncorrelated shadowing function that is also a closed form solution involving error functions, correlation length, surface deviation and incident angles. Because of its simplicity, Smith's shadowing function has often been employed in wave scattering. He et al. [38] developed a light-reflection model in which the reflection distribution is a linear addition of three components: specular, directional and diffuse reflections. In this He et al. model, Smith's shadowing function is employed to account for incoming and outgoing shadowing, and Fresnel relations are used to estimate the fraction of the reflected and absorbed energy. Smith's shadowing function is further approximated by a simple expression [39] without error functions, and this expression has been employed in visual image generation.

Monte Carlo simulations [40] have been used to quantify shadowing models. Those models considered include Wagner's correlated and uncorrelated shadowing functions, Smith's shadowing function, and a model based on Rice's work [41] on random noise. Correlation is considered in this last model; however it involves a summation of an infinite series and numerical integration is required. The results indicate that the model based on Rice's work provides the best agreement with the Monte Carlo solutions, but the numerical integration breaks down for an incident angle greater than approximately 60°.

In this work, a statistical model based on the geometric optics approximation for predicting surface wave scattering is presented. This model uses statistical concepts, rather than bundle tracing employed in the geometric optics approximation. This model includes first-, second- and higher-order scatterings. The formulation of the statistical model is presented in the following section, and the model is quantified through comparisons with electromagnetic theory calculations and with experimental findings in Section 3.

2. Surface wave scattering analysis

2.1. Radiative properties

A semi-transparent surface that is illuminated by an electromagnetic wave will reflect, transmit and absorb different fractions of the incident energy. For perfectly conducting surfaces, all energy is reflected (there is no absorption or transmission). In reality, there is no perfectly conducting material. However, such a scenario can be approximated by many metals. For dielectric materials, on the other hand, significant absorption and transmission occurs. Examples of dielectric materials include metallic oxides and polyimides.

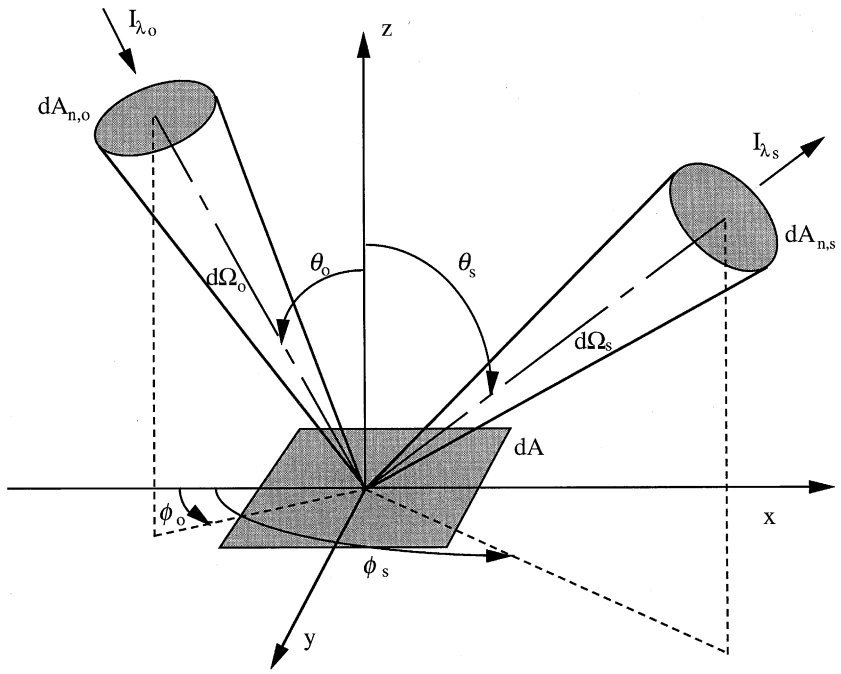

Fig. 1. Bi-directional reflectivity geometry.

To quantify the angular distribution of the reflected energy, the bi-directional reflectivity is defined as π times the ratio of the reflected power per unit solid angle per unit projected area to the incident power [23] and is given as

$$\rho''_\lambda(\Omega_o,\Omega_s)=\left(\frac{\pi}{\cos(\theta_o)}\frac{d\Phi_s}{d\Omega_s}\right)\Big/\left(\frac{d\Phi_o}{d\Omega_o}\right), \tag{1a}$$

where Φ and Ω are the radiant power and solid angle, and the subscripts o and s denote incident and scattering, respectively. Fig. 1 shows the bi-directional reflection geometry in which I_λ is the spectral intensity defined as the radiant power per unit area perpendicular to the direction of travel per unit solid angle and per unit wavelength interval.

Likewise, to describe the angular distribution of the transmitted energy, the bi-directional transmissivity is defined as the ratio of π times the transmitted power per unit solid angle per unit area normal to the direction of transmission to the incident radiant power as

$$\tau''_\lambda(\Omega_o,\Omega_t)=\left(\frac{\pi}{\cos(\theta_o)}\frac{d\Phi_t}{d\Omega_t}\right)\Big/\left(\frac{d\Phi_o}{d\Omega_o}\right), \tag{1b}$$

where the subscript t denotes transmitted quantities. Integration of the bi-directional reflectivity and the bi-directional transmissivity over the respective hemispheres yields the directional reflectivity and transmissivity for a given angle of incidence, respectively. The expressions are

$$\rho'_\lambda(\Omega_o)=\frac{1}{\pi}\int_{2\pi}\rho''_\lambda(\Omega_o,\Omega_s)\cos(\theta_s)\,d\Omega_s \tag{2a}$$

and

$$\tau'_\lambda(\Omega_o)=\frac{1}{\pi}\int_{2\pi}\tau''_\lambda(\Omega_o,\Omega_t)\cos(\theta_t)\,d\Omega_t. \tag{2b}$$

Two additional thermal radiative quantities are the emissivity and absorptivity. These radiative quantities are related by Kirchhoff's law and the conservation of energy [23]. Kirchhoff's law provides the equality between emissivity and absorptivity.

2.2. Random rough surfaces

Two-dimensional random rough surfaces are generated by a stationary stochastic process with a zero mean and a Gaussian probability density function of the surface height [42], $\zeta(\mathbf{r})$. Thus,

$$\langle\zeta(\mathbf{r})\rangle=0, \tag{3a}$$

$$\langle\zeta(\mathbf{r})\zeta(\mathbf{r}')\rangle=\sigma^2\exp\left[-\left(\frac{|x_1-x_2|^2}{\tau_x^2}+\frac{|y_1-y_2|^2}{\tau_y^2}\right)\right], \tag{3b}$$

where $\mathbf{r}$ is the position vector and x, y, z are the components of $\mathbf{r}$. τ_x and τ_y are the correlation lengths in x and y directions, and σ is the mean-square departure of the surface from flatness. The rms slopes in the x-direction and y-direction of these surfaces are given as

$$\langle(\zeta'(x))^2\rangle^{1/2}=\sqrt{2}\sigma/\tau_x, \tag{4a}$$

$$\langle(\zeta'(y))^2\rangle^{1/2}=\sqrt{2}\sigma/\tau_y. \tag{4b}$$

For a given surface, σ and the rms slopes can be determined by measuring the surface height in various locations, then τ_x and τ_y can be found through Eqs. (4a) and (4b). One-dimensional random rough surfaces can be generated by eliminating the y-components and replacing $\mathbf{r}$ by x in Eqs. (3a), (3b) and Eqs. (4a), (4b).

In this work, only two-dimensional random rough surfaces that exhibit no preferential roughness direction are considered; thus τ_x and τ_y are equal and denoted by τ.

2.3. Statistical method

The statistical model is developed based on the geometric optics approximation which provides a multiple scattering solution for random rough surface reflection. In the geometric optics approximation, the energy incident on a rough surface is traced through multiple interactions with the surface until it leaves the surface, and Fresnel reflection is applied to each local point of interaction. In the process of the ray-tracing, an incident bundle may hit the surface once (first-order scattering), twice (second-order scattering) or many more times. Thus, the total energy reflected in the direction of Ω_s is the sum of the reflected energy from all scatterings,

$$\rho''_\lambda(\Omega_o,\Omega_s)=\rho''_{\lambda,1}(\Omega_o,\Omega_s)+\rho''_{\lambda,2}(\Omega_o,\Omega_s)+\rho''_{\lambda,3}(\Omega_o,\Omega_s)+\cdots \tag{5}$$

where the subscripts "1", "2" and "3" denote the first-order, second-order and the third-order scatterings.

For interfaces that are relatively smooth, first-order scattering dominates the surface reflection and very few second-order and higher-order scatterings occur (there is little inter-surface reflection). Thus higher-order scatterings can be neglected so that the bi-directional reflectivity becomes

$$\rho''_\lambda(\Omega_o,\Omega_s)=\rho''_{\lambda,1}(\Omega_o,\Omega_s). \tag{6}$$

Typically, for smooth surfaces with $\sigma/\tau<0.25$, the reflected energy for single scattering is about 95% of the total reflected energy. And for surfaces with an intermediate roughness, $\sigma/\tau<0.5$, the reflected energy is still dominated by first-order scattering (~65%); however, second-order scatterings become considerable (~30%) and contribute to the angular reflection distribution.

2.4. First-order scattering approximation

To understand the statistical approach, this section reviews the single scattering process. Consider a surface that is illuminated by a source with an incident direction of Ω_o. Some portions of the surface may lie in shadowed regions and cannot participate in the scattering process. For the illuminated regions, the energy will be reflected in various directions which depend on the local slopes or local normal vectors. Some of the energy will leave the surface and is considered as a contribution of $\rho''_{\lambda,1}(\Omega_o,\Omega_s)$ while some energy may restrike the surface. The whole process can be interpreted as three probabilities, i.e., the chance that a surface element does not lie in a shadowed area, the fraction of the incoming energy that will be reflected by this element with certain surface slopes, and the chance that the reflected beam leaves the surface. Let *A, B* and *C* denote these three events, and the bi-directional reflectivity is expressed as

$$\rho''_{\lambda,1} \propto P(A \cap B \cap C). \tag{7a}$$

In order to simplify the calculations, the correlation between surface heights and slopes between points is neglected, i.e., events *A, B* and *C* are independent, and the bi-directional reflectivity becomes

$$\rho''_{\lambda,1}(\Omega_o,\Omega_s) \propto P(A)P(B)P(C). \tag{7b}$$

For single scattering, the chance that a surface element does not lie in a shadowed area (event *A*) is equal to the chance that a bundle leaves the surface without restriking the surface (event *C*). Thus, $P(A)$ and $P(C)$ can be expressed by the same notation $S(\Omega,\sigma/\tau,\sigma/\lambda)$, called the shadowing function. For event *A*, $P(A) = S(\Omega_o,\ \sigma/\tau,\sigma/\lambda)$, while for event *C*, $P(C) = S(\Omega_s,\sigma/\tau,\sigma/\lambda)$.

Smith's shadowing function [32] is used in the statistical method because the function provides a simple and reasonably accurate scheme to approximate the influence of shadowing. Smith started from one-dimensional random rough surfaces and approached the shadowing function by using the scenario that bundles leaves a reflection point (event *C*). In addition, correlation between surface heights and surface slopes between points is omitted, leaving the shadowing function independent of σ/λ. Based on this scenario and assumptions, the shadowing function is a function of the incident angle, θ_o, and the surface slope, σ/τ. Smith expressed this function as

$$\begin{aligned} S\left(\theta_s,\frac{\sigma}{\tau}\right) &= \frac{1}{\Lambda+1}, \quad 0^\circ \leqslant \theta_s \leqslant 90^\circ, \\ S\left(\theta_s,\frac{\sigma}{\tau}\right) &= 0, \quad 90^\circ \leqslant \theta_s \leqslant 180^\circ, \end{aligned} \tag{8}$$

where

$$\Lambda = \left[\sqrt{\frac{2}{\pi}}\frac{\sigma_{rms}}{\mu}e^{-(\mu)^2/2\sigma_{rms}^2} - \operatorname{erfc}\left(\frac{\mu}{\sqrt{2}\sigma_{rms}}\right)\right],$$

$\mu = \tan(90^\circ - \theta_s)$, and σ_{rms} is the rms surface slope defined as $\sigma_{rms} = \sqrt{2}\sigma/\tau_x = \sqrt{2}\sigma/\tau_y$. The derivation of the shadowing function involves numerous probability concepts such as conditional probability, subsets, and joint probability density. A detailed description of the formulation of the shadowing function is provided in Ref. [32].

Smith's shadowing function can be adopted in the statistical method for two-dimensional random rough surfaces by simply changing the axes-orientation for each intersection. Suppose that a bundle leaves a reflection point with a scattering direction of $\Omega_s(\theta_s,\phi_s)$. Selecting the projected line of the bundle as the *x*-axis with the origin at the reflection point reduces the two-dimensional shadowing problem to a quasi-one-dimensional problem and the scattering direction becomes $\Omega_s(\theta_s,\phi_s = 0^\circ)$.

For event *B*, $P(B)$ is the fraction of the incident energy that hits an element with certain slopes (ζ_x,ζ_y). Consider a bundle carrying an amount of energy which is proportional to the incident area, A_o, and let $t\left(A_o,\zeta_x,\zeta_y,\theta_o,\sigma/\tau\right)$ denote the transfer function where $t\left(A_o,\zeta_x,\zeta_y,\theta_o,\sigma/\tau\right)\mathrm{d}\zeta_x\mathrm{d}\zeta_y$ [i.e., $P(B)$] is the fraction of that incoming energy which is reflected or transferred by elements with certain slope values (z_x,z_y) within the interval $[\zeta_x - \mathrm{d}\zeta_x/2 \leqslant z_x \leqslant \zeta_x + \mathrm{d}\zeta_x\ /2, \zeta_y - \mathrm{d}\zeta_y/2 \leqslant z_y \leqslant \zeta_y + \mathrm{d}\zeta_y/2]$. To simplify the analysis, the projected line of the bundle is selected as the *x*-axis with the origin at the reflection element. Thus, the scattering direction becomes $\Omega_o(\theta_o,\phi_o = 0^\circ)$. In addition, correlation is neglected between surface heights and surface slopes between points.

To evaluate the transfer function representing the fraction of the incoming energy which is reflected by a surface element with particular slope values (ζ_x,ζ_y), two issues need to be considered: the surface slope distribution and the area ratio. For a Gaussian surface, the surface slope distribution is the multiplication of the slope distributions of ζ_x, and ζ_y as

$$f\left(\zeta_x,\zeta_y,\frac{\sigma}{\tau}\right) = \frac{1}{\sigma_{rms}\sqrt{2\pi}}e^{-\zeta_x^2/2\sigma_{rms}^2}\cdot\frac{1}{\sigma_{rms}\sqrt{2\pi}}e^{-\zeta_y^2/2\sigma_{rms}^2}, \tag{9}$$

where σ_{rms} is the rms surface slope and can be found by $\sigma_{rms} = \sqrt{2}\sigma/\tau$.

Fig. 2 illustrates the contributions of the ratio area on the transfer function. Fig. 2 shows several surface elements which have the same width of Δx but different surface slopes. As shown in Fig. 2(a)–(d), for bundles with an incident angle of θ_o, the bundles can only hit the surface element with a slope between $\zeta_x = -\tan(90^\circ - \theta_o)$ and $\zeta_x = \infty$. Thus, the summation of the transfer

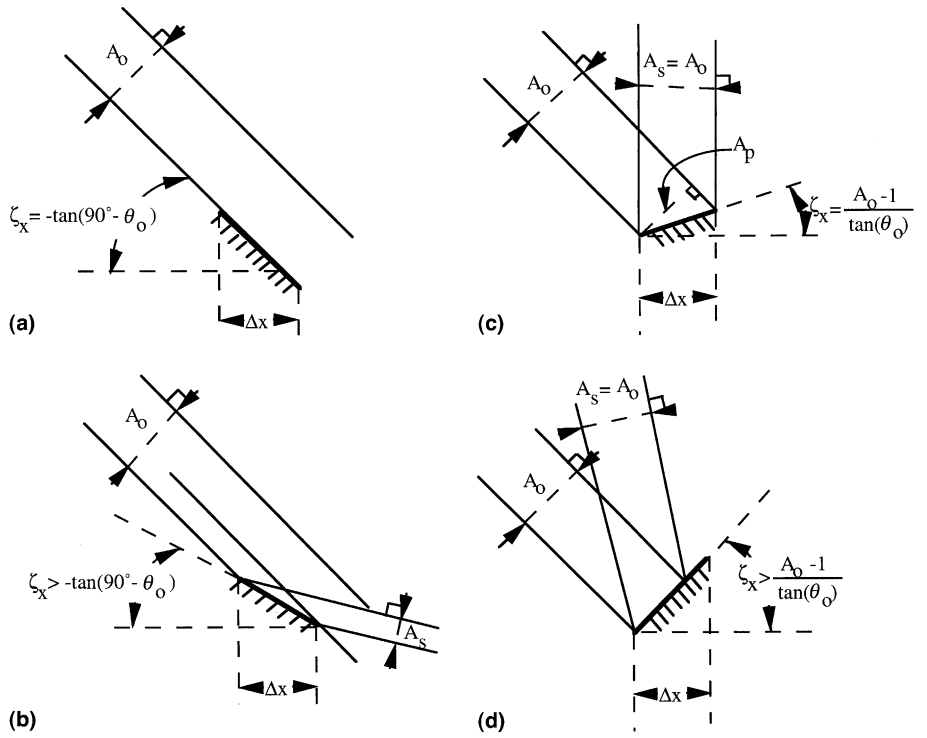

Fig. 2. The transfer function and overshot bundles.

function $t(A_o, \zeta_x, \zeta_y, \theta_o, \sigma/\tau)$ over all such elements which can be hit should be equal to unity.

For the element with a slope of $\zeta_x = -\tan(90° - \theta_o)$ as shown in Fig. 2(a), no energy is reflected and all energy will overshoot the element and hit other surface elements. As the surface slope increases to a less negative value, a portion of the incident energy is reflected, and the remaining energy will overshoot the element and hit other elements (Fig. 2(b)). The amount of energy that is reflected is proportional to the reflecting area, A_s. If the slope is greater than or equal to a particular value $\zeta_x = (A_o - 1)/\tan(\theta_o)$, all incident energy is reflected, and by Snell's law, the reflected area A_s is equal to the incident area A_o (Fig. 2(c) and (d)).

At each overshoot, a fraction of energy is directly reflected and becomes a contribution of the reflection distribution. For the first directly reflected part, the fraction of energy reflected is proportional to the slope distribution weighted by the ratio of the areas of the incident bundle and reflected bundle:

$$t_{1d}(A_o, \zeta_x, \zeta_y, \theta_o, \sigma/\tau) \propto f\left(\zeta_x, \zeta_y, \frac{\sigma}{\tau}\right)\frac{A_s}{A_o}, \tag{10}$$

where the subscripts "1" and "d" denote the first overshoot and the directly reflected part.

Fig. 3 shows an example of the area ratio for the cases with an incident angle of 30° and $A_o = 0.267$. The area ratio is presented from $\zeta_x = -\tan(90° - \theta_o) = -\tan(60°)$ to $\zeta_x = \infty$. For the element with a slope of $-\tan(60°)$ (Fig. 2(a)), A_s is zero, resulting in a zero area ratio. As the slope increases, A_s and the area ratio increase (Fig. 2(b)). For any element that has a slope such that the projected area of the element is greater than A_o, by Snell's law (Fig. 2(c) and (d)), A_s is equal to A_o and the area ratio is unity.

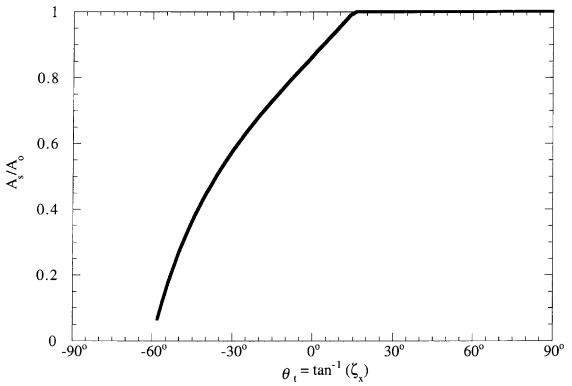

Fig. 3. An example of the area ratio A_s/A_o for $\theta_o = 30°$ and $A_o = 0.267$.

To evaluate the transfer function, $t(A_o, \zeta_x, \zeta_y, \theta_o, \sigma/\tau)$, the overshot bundles need to be considered. For the element with a specific slope of $\zeta_x = -\tan(90° - \theta_o)$, the area of the overshot bundles are the same as that of the original incoming bundles (see Fig. 2(a)). Thus, for this element, energy is distributed exactly as $t_{1d}(A_o, \zeta_x, \zeta_y, \theta_o, \sigma/\tau)$. In addition, the energy carried by these overshot bundles is the maximum energy that overshot bundles can carry. As the slope of the element increases to a less negative value, the overshot bundles carry less energy, and the energy is distributed in a slightly different manner from $t_{1d}(A_o, \zeta_x, \zeta_y, \theta_o, \sigma/\tau)$. As the slope further increases, the energy distribution significantly deviates from $t_{1d}(A_o, \zeta_x, \zeta_y, \theta_o, \sigma/\tau)$; however, the amount of energy carried by the overshot bundles is small. Therefore, the energy distribution of the second directly reflected part, $t_{2d}(A_o, \zeta_x, \zeta_y, \theta_o, \sigma/\tau)$, can be approximated by that of the first directly reflected part, $t_{1d}(A_o, \zeta_x, \zeta_y, \theta_o, \sigma/\tau)$. A similar analogy can be applied to the higher-order directly reflected parts. Thus, the transfer function is a linear summation of $t_{1d}(A_o, \zeta_x, \zeta_y, \theta_o, \sigma/\tau)$ with a weight for each term. Then, factoring $t_{1d}(A_o, \zeta_x, \zeta_y, \theta_o, \sigma/\tau)$ gives

$$t(A_o, \zeta_x, \zeta_y, \theta_o, \sigma/\tau) = t_{1d}(A_o, \zeta_x, \zeta_y, \theta_o, \sigma/\tau) \propto f\left(\zeta_x, \zeta_y, \frac{\sigma}{\tau}\right)\frac{A_s}{A_o}, \tag{11}$$

since the summation of all the weights is unity. The transfer function can be found by normalizing the quantity $f(\zeta_x, \zeta_y, \tau/\sigma)A_s/A_o$ by its integrated value to yield

$$t(A_o, \zeta_x, \zeta_y, \theta_o, \sigma/\tau) = \frac{f(\zeta_x, \zeta_y, \sigma/\tau)\frac{A_s}{A_o}}{\int_{-\infty}^{\infty}\int_{-\tan(90°-\theta_o)}^{\infty} f(\zeta_x, \zeta_y, \sigma/\tau)\frac{A_s}{A_o}\,d\zeta_x\,d\zeta_y}. \tag{12}$$

Note that similar to the shadowing function, $t(A_o, \zeta_x, \zeta_y, \theta_o, \sigma/\tau)$ is not a function of σ/λ because of the assumption that there is no correlation between any elements.

For the first-order scattering, the transfer function $t(A_o, \zeta_x, \zeta_y, \theta_o, \sigma/\tau)$ can be further simplified. For each element with certain slopes (ζ_x, ζ_y), the area of the incoming bundles are set equal to the projected area as shown in Fig. 2(c) [i.e., no overshoot occurs] and the area ratio in Eq. (12) is always unity. The transfer function is then independent of A_o and substituting Eq. (9) into Eq. (12) yields

$$t(\zeta_x, \zeta_y, \theta_o, \sigma/\tau) = e^{-(\zeta_x^2/2\sigma_{z'}^2)}e^{-(\zeta_y^2/2\sigma_{z'}^2)}/\operatorname{erfc}[\tan(90° - \theta_o)]. \tag{13}$$

The term $e^{-(\zeta_x^2/2\sigma_{z'}^2)}e^{-(\zeta_y^2/2\sigma_{z'}^2)}$ results from the slope distribution, and the error function term is the integration of the denominator of Eq. (12).

To complete the specification of $\rho''_{\lambda,1}(\Omega_o, \Omega_s)$, Snell's law is used to relate the incident vector, the scattering vector, and the surface slopes (ζ_x, ζ_y) as

$$\Omega_s = \Omega_o + 2|\Omega_o \cdot \mathbf{n}|\mathbf{n}. \tag{14}$$

As mentioned before, for a given incident direction only one value of the slope pair (ζ_x, ζ_y) yields the desired scattering direction, and the bi-directional reflectivity can be expressed as

$$\rho''_{\lambda,1}(\theta_s, \phi_s) = \frac{\pi}{\cos(\theta_o)}\frac{t(\zeta_x, \zeta_y, \theta_o, \sigma/\tau)\,d\zeta_x\,d\zeta_y}{\sin(\theta_s)\,d\theta_s\,d\phi_s} \times S\left(\theta_o, \frac{\sigma}{\tau}\right)S\left(\theta_s, \frac{\sigma}{\tau}\right)A_p(\zeta_x, \theta_o)F(n, \kappa, \alpha_o), \tag{15}$$

where the first term incorporates energy needed in the definition of the bi-directional reflectivity. $t(\zeta_x, \zeta_y, \theta_o, \sigma/\tau)\,d\zeta_x\,d\zeta_y$ represents the fraction of the incident energy which is reflected by the element, and $\sin(\theta_s)\,d\theta_s\,d\phi_s$ is the solid angle. $S(\theta_o, \sigma/\tau)$ and $S(\theta_s, \sigma/\tau)$ are the incoming and outgoing shadowing functions. $A_p(\zeta_x, \theta_o)$ is the projected area and $F(n, \kappa, \alpha_o)$ is the Fresnel coefficient [23]. α_o is the angle between the incoming bundles, and the surface normal vector $\mathbf{n}$, which is calculated from the surface slopes (ζ_x, ζ_y). Note that the bi-directional reflectivity is a function of $\sigma/\tau, \theta_o, \theta_s$ and ϕ_s, but not λ.

To calculate the first-order scattering, the required input parameters include the surface materials (n,κ), surface geometric parameters σ/τ and the incident direction $\Omega_o(\theta_o, \phi_o = 0°)$. The surface slopes (ζ_x, ζ_y), which yield the desired scattering direction $\Omega_s(\theta_s, \phi_s)$, can be found by Eq. (14). This equation geometrically relates the incident direction, the scattering direction and the surface slopes. In addition, differentiating this equation yields the term $d\zeta_x\,d\zeta_y/d\theta_s\,d\phi_s$. The shadowing and the transfer functions are calculated by Eqs. (8) and (13). The projected area is $A_p(\zeta_x, \theta_o) = 1 + \zeta_x\tan(\theta_o)$ and the Fresnel coefficients depend on surface materials [23].

2.5. Second-order scattering approximation

Similarly, second-order scatterings can be interpreted as probabilities: the chance that a point on the surface does not lie in a shadowed area [event A]; the fraction of the incident energy reflected by an element with certain slopes (ζ_{x1}, ζ_{y1}) [event B]; the chance that the first reflected beam will restrike the surface [event C]; the fraction of the first reflected energy striking an element with certain slopes (ζ_{x2}, ζ_{y2}) [event D]; and the chance that the second reflected beam does not restrike the surface [event E]. Assuming that there is no correlation between surface heights and surface slopes, the second-order scatterings bi-directional reflectivity can be expressed as

$$\rho''_{\lambda,2}(\Omega_o,\Omega_s)\propto P(A)P(B)P(C)P(D)P(E). \tag{16}$$

Events A and B are the same as for single scattering, $P(C)=S(\theta_{s1},\sigma/\tau)$ for single scattering, yet $P(C)=1-S(\theta_{s1},\sigma/\tau)$ for second-order scatterings since $P(C)$ is the probability that the bundles restrike the surface. $P(D)$ can be evaluated in a similar manner as $P(B)$ where the first reflected beam is transformed into the new incident beam. However, for the second-order scattering, the energy (proportional to A_o) carried by the first reflected bundles are fixed. Thus overshoot can occur, and instead of Eq. (13), the general form of the transfer function (Eq. (12)) should be used to evaluate $P(D)$. $P(E)$ is equal to the shadowing function evaluated at the desired scattering angles. Thus,

$$\begin{aligned}
P(A)&=S\Big(\theta_o,\frac{\sigma}{\tau}\Big),\\
P(B)&=t\Big(\zeta_{x1},\zeta_{y1},\theta_o,\frac{\sigma}{\tau}\Big)\,d\zeta_{x1}\,d\zeta_{y1},\\
P(C)&=1-S\Big(\theta_{s1},\frac{\sigma}{\tau}\Big),\\
P(D)&=t\Big(A_o,\zeta_{x2},\zeta_{y2},\theta_{s1},\frac{\sigma}{\tau}\Big)\,d\zeta_{x2}\,d\zeta_{y2},\ \text{and}\\
P(E)&=S\Big(\theta_s,\frac{\sigma}{\tau}\Big).
\end{aligned} \tag{17}$$

For $P(B)$, (ζ_{x1},ζ_{y1}) are the partial derivatives of the surface profile at the first reflection point in directions parallel to and perpendicular to the projected line of the incident bundle, respectively. However, for $P(D)$, (ζ_{x2},ζ_{y2}) are the partial derivatives of the surface profile at the second reflection point in directions parallel to and perpendicular to the projected line of the first reflected bundle.

Similarly, Snell's law is used to geometrically relate the incident vector, slopes of the first reflection point (ζ_{x1},ζ_{y1}), slopes of the second reflection points (ζ_{x2},ζ_{y2}) and the scattering vector. However, unlike single scattering for a given incident direction, more than one combination of (ζ_{x1},ζ_{y1}) and (ζ_{x2},ζ_{y2}) would yield the same desired scattering direction in double scatterings. Thus, let C be a set containing all possible combinations, denoted by

$$\begin{aligned}
C=\big\{&\big[\mathbf{n}_1(\zeta_{x1},\zeta_{y1}),\mathbf{n}_2(\zeta_{x2},\zeta_{y2})\big]:\\
&\Omega_{s1}=\Omega_o+2|\Omega_o\cdot\mathbf{n}_1|\mathbf{n}_1,\Omega_s=\Omega_{s1}+2|\Omega_{s1}\cdot\mathbf{n}_2|\mathbf{n}_2\big\},
\end{aligned} \tag{18}$$

where $\mathbf{n}_1$ and $\mathbf{n}_2$ are the normals of the first reflection point and the second reflection point, and $\Omega_{s1}(\theta_{s1},\phi_{s1})$ is the first reflected vector. Finally, the bi-directional reflectivity of second-order scatterings is

$$\begin{aligned}
\rho''_{\lambda,2}(\theta_s,\phi_s)=&\frac{\pi}{\cos(\theta_o)}\frac{d\zeta_x\,d\zeta_y}{\sin(\theta_s)\,d\theta_s\,d\phi_s}\\
&\times S\Big(\theta_o,\frac{\sigma}{\tau}\Big)S\Big(\theta_s,\frac{\sigma}{\tau}\Big)\int\int_C\Big[1-S\Big(\theta_{s1},\frac{\sigma}{\tau}\Big)\Big]\\
&\times t\Big(\zeta_{x1},\zeta_{y1},\theta_o,\frac{\sigma}{\tau}\Big)t\Big(A_o,\zeta_{x2},\zeta_{y2},\theta_{s1},\frac{\sigma}{\tau}\Big)\\
&\times A_p(\zeta_x,\theta_o)F(n,\kappa,\alpha_o)F(n,\kappa,\alpha_{s1})d\zeta_{x1}d\zeta_{y1}.
\end{aligned} \tag{19}$$

To calculate the second-order scattering bi-directional reflectivity, surface properties, surface geometric parameters and incident directions are required. The term $d\zeta_x\,d\zeta_y/d\theta_s\,d\phi_s$ can be found by differentiating Eq. (14). Eqs. (8) and (12) are used to evaluate the shadowing functions and the transfer functions. The projected area is $A_p(\zeta_x,\theta_o)=1+\zeta_x\tan(\theta_o)$. $F(n,\kappa,\alpha_o)$ and $F(n,\kappa,\alpha_{s1})$ are Fresnel coefficients for each surface reflection. $F(n,\kappa,\alpha_o)$ accounts for the fraction of incident energy in the first reflected bundles, and $F(n,\kappa,\alpha_{s1})$ accounts for the fraction of the energy in the first reflected bundles to second reflected bundles. α_o is the angle between the incident bundle and $\mathbf{n}_1$, while α_{s1} is the angle between the first reflected bundle and $\mathbf{n}_2$.

The second-order scattering bi-directional reflectivity is a function of $\sigma/\tau,\theta_o,\theta_s$ and ϕ_s. However, unlike single scattering, $\rho''_{\lambda,2}(\theta_s,\phi_s)$ cannot be expressed in an algebraic formula. A numerical evaluation is required for the evaluation of the double integral in Eq. (19) over the domain C (Eq. (18)).

To avoid this integration, the second-order scattering can be approximated in a simpler form. The concept used to simplify the second-order approximation is to assume all reflected energy is concentrated in several dominant directions. Consider the fraction of the incoming energy in a specified direction after the first-order scattering from the surface, e'_1. This includes energy that will leave the surface (first-order scattering) and the energy that will restrike the surface (second and higher-order scatterings). Thus, subtracting the transmissivity from unity yields

$$e'_1=1-\tau'_{\lambda,1}(\theta_o). \tag{20}$$

The prime denotes e'_1 is a directional quantity. For a perfectly conducting surface, $\tau'_{\lambda,1}(\theta_o)=0$ and e'_1 is equal to unity. Similarly, e'_2 is the fraction of the incoming energy after the second-order scattering and

$$e'_2=1-\tau'_{\lambda,1}(\theta_o)-\rho'_{\lambda,1}(\theta_o)-\tau'_{\lambda,2}(\theta_o). \tag{21}$$

Note that the hemispherical reflectivity and transmissivity can be found by Eqs. (2a) and (2b). Consider the angular distribution of e'_1, the fraction of the incoming energy which is reflected by an element into a particular direction after the first scattering from the surface, e''_1. The result is

$$e''_1=S\Big(\theta_o,\frac{\sigma}{\tau}\Big)A_p(\zeta_x,\theta_o)t\Big(\zeta_{x1},\zeta_{y1},\theta_o,\frac{\sigma}{\tau}\Big)F(n,\kappa,\alpha_o). \tag{22}$$

The quantity depends upon the incident and scattering directions; therefore, the quantity has a double prime. Multiplying e''_1 with the outgoing shadowing function $S(\theta_s,\sigma/\tau)$ yields the fraction of the incoming energy of

first-order scattering, and an additional angle and slope factor yields the bi-directional reflectivity for first-order scattering in Eq. (19). On the other hand, multiplying e_1'' by one minus the outgoing shadowing function, $1 - S(\theta_s, \sigma/\tau)$, yields the fraction of the incoming energy that restrikes the surface and becomes second and higher-order scatterings.

To further simplify the expression, the energy in all directions is assumed to be divided among four quadrants formed by the planes $\phi_s = 0°$ and $\phi_s = 90°$. Energy within each quadrant is first assumed to be reflected within one plane of ϕ_s. Then within that plane, all energy is assumed to be reflected in one polar direction. Thus, there are four reflected bundles, and this second-order scattering problem becomes four first-order scatterings. The key issue in this approximation is to estimate the amount of energy carried by each bundle as well as their reflection directions. One way to determine the amount of energy carried by each bundle is integrating the area under the curve $e_1''[1 - S(\theta_s, \sigma/\tau)]$ over its quadrant. Also, the reflected direction of each bundle can be approximated by its mean value (weighted by energy distribution).

The bundles' reflected directions and the fraction of the incoming energy they contain can be further approximated. Fig. 4 presents $1 - S(\theta_s, \sigma/\tau), e_1''$ and $e_1''[1 - S(\theta_s, \sigma/\tau)]$ as a function of the first scattering angle, θ_{s1}, for a one-dimensional perfectly conducting random rough surface with a surface slope of 0.75. These results are generated by Eqs. (8) and (22). The incident angle is 30°. $1 - S(\theta_s, \sigma/\tau)$ is the chance that the bundles reflected at this first scattering angle will restrike the surface. As shown in Fig. 4, bundles with a scattering angle of 0° will leave the surface, while bundles with a reflected angle greater than 90° will restrike the surface.

The distribution of e_1'' is dependent on the incident angle, θ_o, and the projected area, $A_p(\zeta_x, \theta_o)$. e_1'' has an asymmetric distribution and a large amount of energy is reflected in negative scattering angles. The fraction of the incoming energy that will restrike the surface, $e_1''[1 - S(\theta_s, \sigma/\tau)]$, consists of a region centered approximately at a scattering angle of $\theta_s = -90°$ and another region centered at about $\theta_s = 90°$. The first region has a peak magnitude about twice as great as that of the second. In addition, as shown in Fig. 4, the peak of the positive region is located at approximately 90°. This is because $1 - S(\theta_s, \sigma/\tau)$ is increasing as $|\theta_s|$ increases from zero and reaches unity when $\theta_s \geqslant 90°$, while e_1'' is decreasing as $\theta_s > 90°$. A similar situation is observed for the negative region such that the reflected polar angles of the bundles can be approximated at 90° and −90°. This approximation has been determined to be accurate for surfaces with a surface slope less than 1.2.

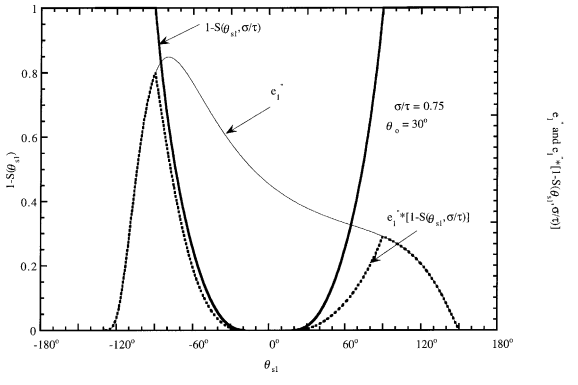

Fig. 4. Shadowing function and energy distribution.

Even though the fraction of the incoming energy that restrikes the surface shown in Fig. 4 is for a one-dimensional case, a similar two-region curve applies to two-dimensional cases. For any particular ϕ_s, the shadowing function is independent of ϕ_s.

For an element with a zero slope with respect to y-axis ($\zeta_y = 0$), the energy will be reflected in the plane of incidence $\phi_o = \phi_s = 0°$. As ζ_y varies, energy will be reflected out of the incident plane. The reflected energy distribution over ϕ_s has a geometric relationship with the Gaussian distribution of ζ_y. Thus, the azimuthal angles of the bundles can be approximated by $2\tan(\zeta_{y,m})$. The tangent function and the factor of two result from the geometric relationship, and $\zeta_{y,m}$ is the mean of all possible ζ_y values that reflect energy to one quadrant. This value is $\zeta_{y,m} = \pm\sqrt{2/\pi}\sigma_{rms}$. Let $\Omega_I, \Omega_{II}, \Omega_{III}$ and Ω_{IV} be the reflection directions of these four bundles:

$$\begin{aligned}
\Omega_I &= \Omega(\theta_s, \phi_s) = \Omega\big(90°, 2\tan(\zeta_{y,m})\big),\\
\Omega_{II} &= \Omega(\theta_s, \phi_s) = \Omega\big(90°, -2\tan(\zeta_{y,m})\big),\\
\Omega_{III} &= \Omega(\theta_s, \phi_s) = \Omega\big(-90°, 2\tan(\zeta_{y,m})\big), \text{ and}\\
\Omega_{IV} &= \Omega(\theta_s, \phi_s) = \Omega\big(-90°, -2\tan(\zeta_{y,m})\big).
\end{aligned} \tag{23}$$

According to the conservation of energy, the fraction of the incoming energy which will restrike the surface after hitting the surface once (i.e., the summation of the energy contained in the regions) is $1 - \rho'_{\lambda,1}(\theta_o) - \tau'_{\lambda,1}(\theta_o)$. Then, the fraction of the incoming energy carried by each bundle can be approximated by this total energy that will restrike the surface weighted by the magnitudes of $e_1'[1 - S(\theta_s, \sigma/\tau)]$ evaluated at the reflection angles of the four bundles. To simplify the notation, let $r(\Omega, \sigma/\tau) = e_1'(\theta_s)[1 - S(\theta_s, \sigma/\tau)]$, and the fraction of the incoming energy carried by the bundle reflected at the scattering direction of Ω_I is estimated as follows:

$$e_I(\Omega_I, \sigma/\tau) = \frac{\left[1 - \rho'_{\lambda,1}(\theta_o) - \tau'_{\lambda,1}(\theta_o)\right] r(\Omega_I, \sigma/\tau)}{r(\Omega_I, \sigma/\tau) + r(\Omega_{II}, \sigma/\tau) + r(\Omega_{III}, \sigma/\tau) + r(\Omega_{IV}, \sigma/\tau)}. \tag{24}$$

For the reflection directions Ω_{II}, Ω_{III} and Ω_{IV}, $e_{II}(\Omega_{II},\sigma/\tau)$, $e_{III}(\Omega_{III},\sigma/\tau)$, $e_{IV}(\Omega_{IV},\sigma/\tau)$ are obtained by replacing the argument $r(\Omega_I,\sigma/\tau)$ by $r(\Omega_{II},\sigma/\tau)$, $r(\Omega_{III},\sigma/\tau)$ and $r(\Omega_{IV},\sigma/\tau)$, respectively, in the numerator of Eq. (24). The bi-directional reflectivity of the second-order scattering can be estimated

$$\rho''_{\lambda,2}(\theta_s,\phi_s)=\frac{\pi}{\cos(\theta_o)}\frac{d\zeta_x\,d\zeta_y}{\sin(\theta_s)\,d\theta_s\,d\phi_s}\times S\left(\theta_o,\frac{\sigma}{\tau}\right)S\left(\theta_s,\frac{\sigma}{\tau}\right)\sum_{j=I,II,III,IV}e_j(\Omega_I,\sigma/\tau)\times t\left(A_o,\zeta_{x2},\zeta_{y2},\theta_{jI},\frac{\sigma}{\tau}\right)A_p(\zeta_x,\theta_o)F(n,\kappa,\alpha_{s1}). \tag{25}$$

Comparing Eq. (19) to Eq. (25), the first few terms are the same, while the integral in Eq. (19) is replaced by a four-time summation. To compute the bi-directional reflectivity based on Eq. (25), the reflected directions of the four bundles are required and can be found by Eq. (22). The fraction of the incoming energy in the bundles is then evaluated by Eq. (24). Once the reflected angles and the energy of the bundles are solved, the calculation steps are similar to that of first-order scatterings.

2.6. Higher-order scattering approximation

For the surface with a surface slope less than 1.1, the energy involved in the third and higher-order scattering is typically less than a tenth of the total incident energy, and in general, the energy reflected is relatively diffuse. In this work, the reflected energy for the higher-order scatterings is simply assumed to follow a cosine distribution with its peak at the anti-scattering angle weighted by the amount of energy involved in the third and higher-order scatterings.

$$\rho''_{\lambda,H}(\theta_s,\phi_s)=\frac{\left[1-\rho'_{\lambda,1}(\theta_o)-\tau'_{\lambda,1}(\theta_o)-\rho'_{\lambda,2}(\theta_o)-\tau'_{\lambda,2}(\theta_o)\right]}{2\pi[\sin(\theta_o)-\cos(\theta_o)]}\times\cos(\theta_s+\theta_o)\frac{\pi}{\cos(\theta_o)}. \tag{26}$$

Eqs. (2a) and (2b) is used to calculate the hemispherical reflectivity and the transmissivity reflectivity.

Finally, the bi-directional reflectivity can be found by adding the bi-directional reflectivity for first-order scattering, Eq. (15), second-order scattering, Eq. (25), and higher-order scatterings, Eq. (26).

3. Results and comparisons

3.1. One-dimensional random rough surfaces

Fig. 5 presents bi-directional reflection results predicted by the statistical model for one-dimensional perfectly conducting random rough surfaces. The results include first-order, second-order, higher-order and total bi-directional reflectivities. The results predicted by the geometric optics approximation and the electromagnetic theory are also presented for comparison. The electromagnetic theory solution is obtained by transforming Maxwell's equations into surface integrals, and the integral equations are discretized into matrix forms. LAPACK-b1 routines on a Cray Y-MP4/464 are used to solve the matrix and determined the reflection distribution [10,11]. Each surface length is discretized into at most 2450 points, depending on the roughness of the surface. Surface lengths are typically 100–200λ. The surface length is made as long as possible to minimize the edge effects. For the geometric optics approximation, each surface length is represented by at most 2000 nodes and surface lengths are typically 100–200λ [30,31].

Fig. 5(a) presents the results for a surface that is relatively smooth ($\sigma/\tau=0.2$). The incident angle is $\theta_o=30°$ and the bi-directional reflectivity is presented for scattering angles, θ_s, between $-90°$ and $90°$. For this case, the reflected energy for the first-order scattering is about 98% of the total energy. The exact and approximate results are a Gaussian-shaped curve about the scattering angle, $\theta_s=\theta_o$. The reflection distribution spans a range of scattering angles, but the distribution does not spread over the entire hemisphere. The bi-directional reflectivity for the surface with an intermediate roughness of $\sigma/\tau=0.5$ is shown in Fig. 5(b). For this case, although the total reflection is still dominated by the first order scattering, the second-order scattering becomes considerable and has an important contribution to the total reflection. In general, the total reflection distribution spans a larger angular region than the case presented in Fig. 5(a). The energy is reflected more diffusely throughout the hemisphere, and no significant peaks occur. Both approximate predictions and the exact solutions are in good agreement for these two cases.

The reflection results for very rough surfaces are illustrated in Fig. 5(c) and (d) with $\sigma/\tau=0.75$ and $\sigma/\tau=1.1$, respectively. For the case with $\sigma/\tau=0.75$, the total reflection has equal contribution from the first-order and second-order scatterings. Both approximate models and the electromagnetic theory predict a very diffuse total reflection distribution with a slight enhancement in the angular region about $\theta_s=\theta_o=30°$. The slight enhancement is due to the second-order scattering. For the case with $\sigma/\tau=1.1$ with rms deviation on the order of the correlation length, the first and second-order scattering dominate the total reflection distribution. The geometric optics approximation shows that a large amount of energy for the higher-order scattering is reflected at the anti-scattering angle of $\theta_s=-\theta_o=-30°$, resulting in a retro-reflection peak in the total reflection distribution. However, no retro-reflection peak is predicted by the statistical method.

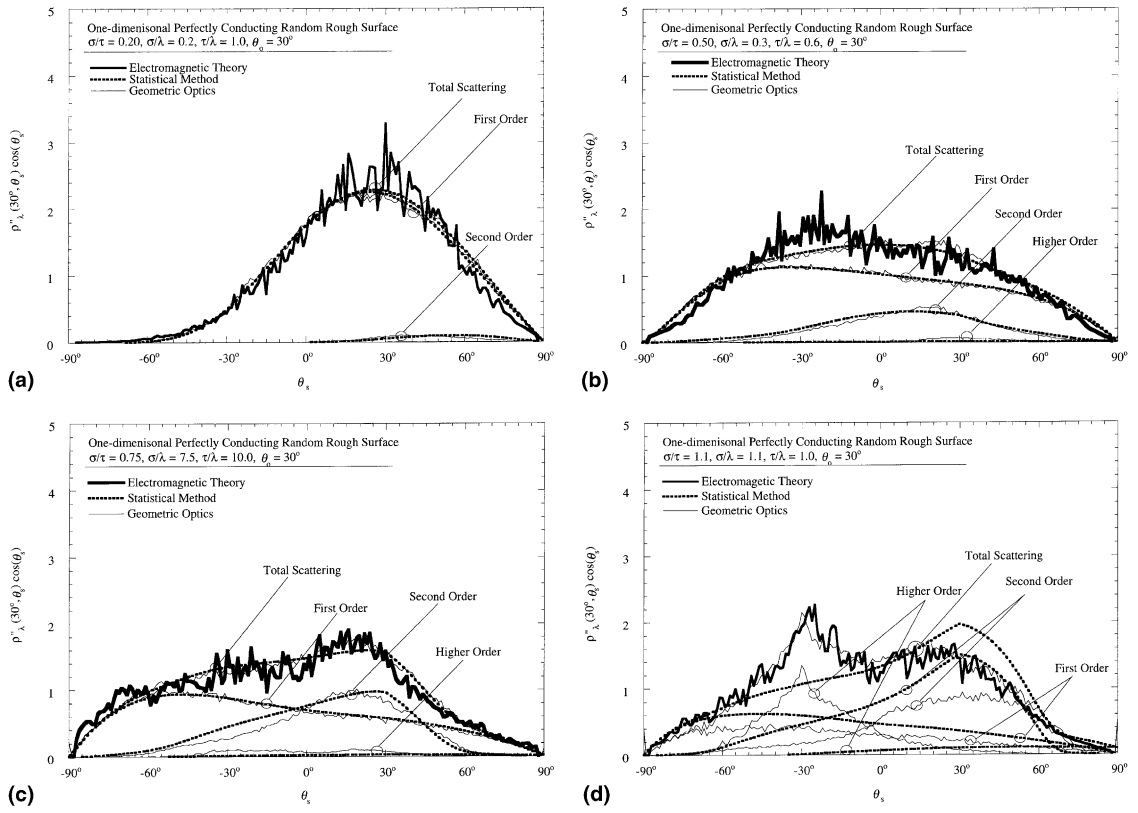

Fig. 5. Comparisons of approximate predictions and electromagnetic theory calculations for perfectly conducting surfaces: (a) $\sigma/\tau = 0.2,\ \sigma/\lambda = 0.2,\ \tau/\lambda = 1.0,\ \theta_o = 30°$; (b) $\sigma/\tau = 0.5,\ \sigma/\lambda = 0.3,\ \tau/\lambda = 0.6,\ \theta_o = 30°$; (c) $\sigma/\tau = 0.75,\ \sigma/\lambda = 7.5,\ \tau/\lambda = 10.0,\ \theta_o = 30°$; (d) $\sigma/\tau = 1.1,\ \sigma/\lambda = 1.1,\ \tau/\lambda = 1.0,\ \theta_o = 30°$.

The parameter domain of validity for the geometric optics approximation has been constructed based on a directional energy criterion [30]. The criterion, E_d, is defined as the ratio of the difference in directional reflected energy predicted by the exact solution and by the approximation within an angular region $\Delta\theta_s$ to the averaged incident energy predicted by the exact solution. The ratio is evaluated over all directions in the hemisphere and the average difference is used in the criterion.

In this work, the parameter domains of validity for the statistical method are also constructed based on this directional energy criterion. For a rather restrictive comparison, in this work, $\Delta\theta_s = 1°$ and the approximation is considered valid if $E_d < 0.20$. Both the exact solution and the geometric optics approximation conserve energy within 1%. Approximately 40 different surfaces were compared to construct the domain of validity, with the correlation lengths ranging from $\tau/\lambda = 0.1$ to $\tau/\lambda = 10.0$. The range of rms deviation is from $\sigma/\lambda = 0.1$ to $\sigma/\lambda = 10.0$, corresponding to a range of the ratio σ/τ from 0.01 to 4.0. A majority of the calculations were performed in the regions near the domain boundaries. Over 60 surface realizations were used for both the exact predictions and the geometric optics approximation. Due to computational limitations, the exact solution is inaccurate at incident angles larger than 45°, since conservation of energy for such surfaces diverges. Therefore, the results at incident angles larger than 45° are not reported.

Fig. 6 illustrates the domain of validity of the statistical model. The domain of the geometric optics approximation is also presented for comparison. The domain of validity of the statistical method model based on the directional criterion has a similar shape as that of the geometric optics approximation. It is vertically and horizontally bounded by $(\sigma/\lambda)\cos\theta_o = 0.20$ and $\sigma/\tau = 1.0$. Note that the entire region for which the statistical method model is valid is covered by the region for the geometric optics approximation. This suggests that the assumption of no correlation between surface slopes and surface heights between points is inadequate for cases with a σ/τ approximately greater than 1.0. However, the domain of validity of the statistical method model has already covered an important range of surface parameters of interest in engineering purposes.

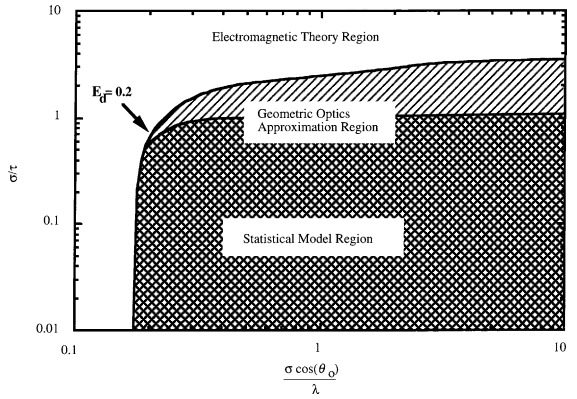

Fig. 6. Rough surface scattering domains of validity for one-dimensional surfaces. The range of parameters compared includes $0.01 \leqslant \sigma/\tau \leqslant 10.0$, $0.1 \leqslant \sigma/\lambda \leqslant 10.0$ and $-45° \leqslant \theta_o \leqslant 45°$.

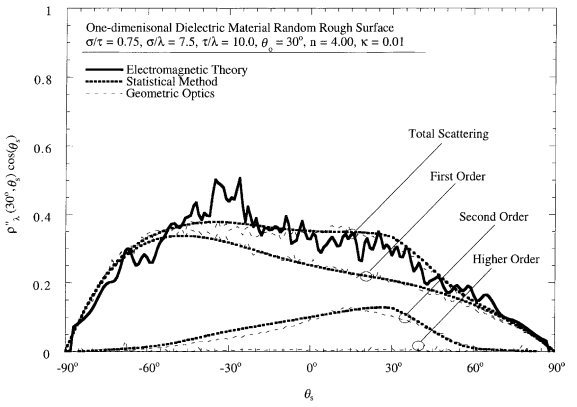

Fig. 7. Comparisons of approximate prediction with electromagnetic theory calculations for dielectric materials. $\sigma/\tau = 0.75$, $\sigma/\lambda = 7.5$, $\tau/\lambda = 10.0$, $\theta_o = 30°$, $n = 4.00$, $\kappa = 0.01$.

One-dimensional dielectric material surfaces are also considered. Fig. 7 illustrates the reflection distribution for a dielectric material with optical constants $(n, \kappa) = (4, 0.01)$ and with the same geometric parameters as the perfectly conducting case presented in Fig. 5(c), where $\sigma/\tau = 0.75, \sigma/\lambda = 7.5$ and $\tau/\lambda = 10.0$. Similarly, the first-order, second-order, higher-order and total bi-directional reflectivities are presented for both approximate predictions, and the results are compared with the electromagnetic theory calculations. Comparison of the dielectric material results with the perfectly conducting surface reflectivity results indicates a three-fold decrease in magnitude of the total reflection distribution, and the shape of the reflection distribution curve changes. More energy is reflected in the negative scattering angle region for the dielectric material. This phenomenon occurs because a fraction of energy is absorbed after each bundle–surface interaction for the dielectric material (the rest of the energy is transmitted through the surface interface). As a result of the absorption for the dielectric material, the reflected energy for the second-order scattering is significantly lower in magnitude relative to the reflected energy for the first-order scattering. For the perfectly conducting surface, the energy distributions for the first and second-order scatterings are of comparable magnitude. In general, as shown in Fig. 7, the approximate solutions and the electromagnetic theory calculation are in good agreement.

Several dielectric cases have been studied and compared to the perfectly conducting surfaces. For both the geometric optics and statistical method approximation, the domain of application for perfectly conducting surfaces ($E_d < 0.20$) should be a conservative estimate for dielectric materials. For smooth surfaces, the values of E_d both for dielectric and for perfectly conducting cases are very similar. For rough surfaces, the approximations are slightly more accurate for dielectric cases than perfectly conducting cases. In general, the values of E_d for dielectric surfaces are lower than for perfectly conducting surfaces for rough and very rough cases. The approximations should be more accurate for dielectric cases since the second and third-order scatterings dominate the solution for a perfectly conducting rough surface. For dielectric materials, only a fraction of the incident energy is reflected after each scattering and the energy in the higher-order scatterings is smaller than single scatterings. The surface reflection is then dominated by single scattering.

The exact solution for dielectric surfaces takes approximately 100 megawords of memory and 14 h of CPU time using the electromagnetic theory to predict the averaged scattering from 60 very rough surface realizations. The geometric optics approximation takes approximately one-hundredth of the memory and one-tenth of the CPU time to predict the scattering, while the required CPU time and memory for the statistical method are approximately one-hundredth that of the geometric optics approximation.

3.2. Two-dimensional random rough surfaces

For two-dimensional surfaces, since extensive exact solutions are not presently available, the approximate models are quantified by comparisons with data from existing experimental results from various experimental facilities. Comparisons of the statistical method predictions and geometric optics solutions with various existing experimental findings [21,22,31,33,42–45] are made, and selected results are presented in Fig. 8. In Fig. 8, the results are presented in ascending order of surface slope for curves (a)–(f). The results are shown in the plane of incidence, $\phi_o = 0°$. The vertical axis is the normalized bi-directional reflectivity [and multiplied by $\cos(\theta_s)$]. The

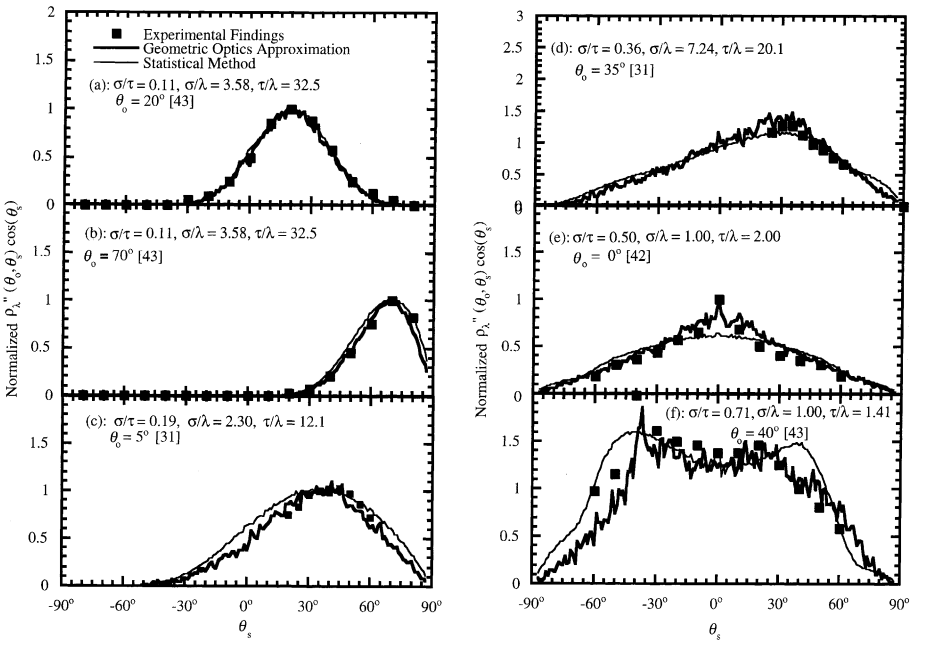

Fig. 8. Comparison of the geometric optics approximation and the statistical method with existing experimental findings for the normalized bi-directional reflectivity.

approximate predictions are shown with solid lines and experimental findings shown with specific points.

Curves (a)–(c) in Fig. 8 illustrate the results from smaller roughness surfaces ($\sigma/\tau < 0.25$). In these cases, the geometric optics predictions, the statistical method solutions and the experimental findings are Gaussian-shaped curves around the scattering angles, and the reflection distribution spans a limited range of scattering angles. No distinct off-specular peaks are noticed in curves (a) and (b). For curve (c), the maximum values of the reflection distribution occur at angles greater than the specular angles. In general, these approximate predictions are in excellent agreement with the experimental findings. The rms errors for the geometric optics approximation and for the statistical method are less than 0.10 for curves (a), (b) and (c). Other researchers [43] had compared these experimental findings with the approximate methods such as the Kirchhoff approximation, and such approximate methods are in less accurate agreement in both trend and magnitude than the geometric optics and statistical method results.

The results from surfaces with intermediate roughness ($0.25 < \sigma/\tau < 0.70$) are presented in curves (d) and (e). The reflection distribution is no longer a Gaussian-shaped curve and the distribution spreads over the entire hemisphere. For case (d), an off-specular peak is also observed for all the predictions. Unlike case (c), the maximum values are at angles smaller than the specular angles. The agreement between the experimental findings and approximate results is excellent. The rms errors for the geometric optics approximation and the statistical method are less than 0.15. For the very rough surface shown in curve (f), a slight retro-reflection peak is observed in the geometric optics prediction and the experimental findings. At an incident angle of 40°, a sharp peak occurs at $\theta_s = -40°$ and a smaller forward peak occurs at $\theta_s = 20°$. Compared with the experimental data, the statistical method does not predict a strong retro-reflection peak at the anti-scattering angle; in general, the predictions agree in trend with the experimental findings and provide a fair approximation on magnitude. The rms error and the maximum error are approximately 0.22 and 0.48 for the statistical method. The geometric parameters for all the cases including both experimental and numerical studies compared in this work are within the domains of validity of the one-dimensional geometric optics approximation and statistical method. In summary, since the two-dimensional geometric optics predictions agree well with all the existing approaches, it seems likely that the one-dimensional domain is valid for two-dimensional surfaces. For the statistical model, the comparisons indicate that this approximation is a relatively inexpensive tool for surfaces with a σ/τ less than 0.5. In addition, the statistical model provides a fair approximation on both magnitude and trend for the surfaces with a σ/τ greater than 0.5.

The geometric optics and statistical model predictions are also compared with a few existing electromagnetic theory calculations [15,21,22]. Similarly, the geometric optics predictions and electromagnetic theory

calculations are found to be very similar for a large range of σ/τ, and for the statistical model, the two-dimensional surface domain is smaller than the one-dimensional domain.

4. Conclusions

The statistical model is developed based on the geometric optics approximation. Instead of tracing the bundles, probability and statistical concepts are applied to quantify the ray-tracing process. The total bi-directional reflectivity including the first-, second- and higher-order scatterings can be expressed in a closed form. The basic elements of this model are the incoming and outgoing shadowing functions, the transfer function and the Fresnel coefficient. The bi-directional reflectivity is a function of geometric parameters, dielectric properties and incident angles but not the incident wavelength because no correlation between surface heights and slopes is assumed.

For one-dimensional random rough surfaces, the statistical model is quantified by the exact electromagnetic theory. It has been shown that the statistical method can provide accurate results for surfaces which have a σ/τ less than or equal to unity for one-dimensional surfaces and its domain covers the majority of engineering problems. In addition, unlike the geometric optics approximation, no surface generation is required for the statistical model and the computational time and memory units are one-hundredth of those required by the geometric optics approximations.

General two-dimensional surface electromagnetic theory calculations are not presently available; thus the statistical model is quantified by the experimental data from various facilities and by the few existing electromagnetic theory calculations. The comparisons indicate that the statistical model is a relatively inexpensive approach for surface reflection distribution predictions from surfaces with a σ/τ less than 0.5, and this model can provide an approximation on both magnitude and trend for the surfaces with a σ/τ greater than 0.5.

Acknowledgements

The authors acknowledge the support of the National Science Foundation, under Grant NSF CTS 95-31772, and the National Center for Supercomputing Applications.

References

[1] M.N. Vesperinas, J.A.S. Gil, Light scattering from a random rough interface with total internal reflection, J. Opt. Soc. Am. A 9 (1992) 424–436.

[2] V. Celli, A.A. Maradudin, A.M. Marvin, A.R. McGurn, Some aspects of light scattering from a randomly rough metal surface, J. Opt. Soc. Am. A 2 (1985) 2225–2239.

[3] J.M. Soto-Crespo, M. Nieto-Vesperinas, Electromagnetic scattering from very rough random surfaces and deep reflection gratings, J. Opt. Soc. Am. A 6 (1989) 367–384.

[4] A.A. Maradudin, T. Michel, A.R. McGurn, E.R. Mendez, Enhanced backscattering of light from a random grating, Ann. Phys. 203 (1990) 255–307.

[5] A.A. Maradudin, J.Q. Lu, T. Michel, T.H. Gu, J.C. Dainty, A.J. Sant, E.R. Mendez, M.N. Vesperinas, Enhanced backscattering and transmission of light from random surfaces on semi-infinite substrates and thin films, Waves Random Media 3 (1991) S129–141.

[6] A.A. Maradudin, E.R. Mendez, T. Michel, Backscattering effects in the elastic scattering of *p*-polarized light from a large-amplitude random metallic grating, Opt. Lett. 14 (1989) 151–153.

[7] A.R. McGurn, A.A. Maradudin, An analogue of enhanced backscattering in the transmission of light through a thin film with a randomly rough surface, Opt. Comm. 72 (1989) 279–285.

[8] P. Phu, A. Ishimaru, Y. Kuga, Controlled millimeter-wave experiments and numerical simulations on the enhanced backscattering from one-dimensional very rough surface, Radio Sci. 28 (1993) 533–548.

[9] J.A.S. Gil, M.N. Vesperinas, Light scattering from random dielectric surfaces, J. Opt. Soc. Am. A 8 (1991) 1270–1286.

[10] R.A. Dimenna, R.O. Buckius, Microgeometrical contour contributions to surface scattering, Thermal Sci. Eng. 2 (1994) 166–171.

[11] R.A. Dimenna, R.O. Buckius, Electromagnetic theory predictions of the directional scattering from triangular surfaces, J. Heat Transfer 116 (1994) 639–645.

[12] Z.H. Gu, J.Q. Lu, A.A. Maradudin, A. Martinez, Enhanced backscattering from a free-standing dielectric film, Appl. Opt. 34 (1995) 3529–3534.

[13] Z.H. Gu, J.Q. Lu, A. Martinez, E.R. Mendez, A.A. Maradudin, Enhanced backscattering from a one-dimensional rough dielectric film on a glass substrate, Opt. Lett. 19 (1994) 604–606.

[14] A. Madrazo, M.N. Vesperinas, Scattering of electromagnetic waves from a cylinder in front of a conducting plane, J. Opt. Soc. Am. A 12 (1995) 1298–1309.

[15] C. Macaskill, B.J. Kachoyan, Iterative approach for the numerical simulation of scattering from one- and two-dimensional rough surfaces, Appl. Opt. 32 (1993) 2839–2847.

[16] P. Tran, A.A. Maradudin, Scattering of a scalar beam from a two-dimensional randomly rough hard wall: Dirichlet and Neumann boundary conditions, Appl. Opt. 32 (1993) 2848–2851.

[17] P. Tran, A.A. Maradudin, The scattering of electromagnetic waves from a randomly rough 2D metallic surface, Opt. Comm. 110 (1994) 269–273.

[18] P. Tran, V. Celli, A.A. Maradudin, Electromagnetic scattering from a two-dimensional, randomly rough, perfectly conducting surface: iterative methods, J. Opt. Soc. Am. A 11 (1994) 1686–1689.

[19] L. Tsang, C.H. Chan, K. Pak, Backscattering enhancement of a two-dimensional random rough surface (three-dimen-

sional scattering) based on Monte Carlo simulations, J. Opt. Soc. Am. A 11 (1994) 711–715.
[20] L. Tsang, C.H. Chan, K. Pak, H. Sangani, A. Ishimaru, P. Phu, Monte Carlo simulations of large-scale composite random rough-surface scattering based on the banded-matrix iterative approach, J. Opt. Soc. Am. A 11 (1994) 691–696.
[21] K. Pak, L. Tsang, H. Chan, J. Johnson, Backscattering enhancement of electromagnetic waves from two-dimensional perfectly conducting random rough surfaces based on Monte Carlo simulations, J. Opt. Soc. Am. A 12 (1995) 2491–2499.
[22] J. Johnson, L. Tsang, R.T. Shin, K. Pak, C.H. Chan, A. Ishimaru, Y. Kuga, Backscattering enhancement of electromagnetic waves from two-dimensional perfectly conducting random rough surfaces: a comparison of Monte Carlo simulations with experimental data, IEEE Trans. Ant. Prop. 44 (1996) 748–755.
[23] M.Q. Brewster, Thermal Radiative Transfer and Properties, Wiley, New York, 1992.
[24] M.F. Modest, Radiative Heat Transfer, McGraw-Hill, New York, 1993.
[25] P. Beckmann, A. Spizzichino, The Scattering of Electromagnetic Waves from Rough Surfaces, Pergamon Press, Oxford, 1963.
[26] M.F. Chen, A.K. Fung, A numerical study of the regions of validity of the Kirchhoff and small-perturbation rough surface scattering models, Radio Sci. 23 (1988) 163–170.
[27] E. Thorsos, The validity of the Kirchhoff approximation for rough surface scattering using gaussian roughness spectrum, J. Acoust. Soc. Am. 83 (1988) 78–92.
[28] M.N. Vesperinas, J.A.S. Gil, Light transmission from a randomly rough dielectric diffuser: theoretical and experimental results, Opt. Lett. 15 (1990) 1261–1263.
[29] R.A. Dimenna, R.O. Buckius, Quantifying specular approximations for angular scattering from perfectly conducting random rough surfaces, J. Thermophys. Heat Transfer 8 (1994) 393–399.
[30] K. Tang, R.A. Dimenna, R.O. Buckius, Regions of validity of the geometric optics approximation for angular scattering from very rough surfaces, Int. J. Heat Mass Transfer 40 (1997) 49–59.
[31] K. Tang, R.O. Buckius, The geometric optics approximation for reflection from two-dimensional random rough surfaces, Int. J. Heat Mass Transfer 41 (1998) 2037–2047.
[32] B.G. Smith, Geometrical shadowing of a random rough surface, IEEE Trans. Ant. Prop. 15 (1967) 668–671.
[33] R.J. Wagner, Showing of randomly rough surfaces, J. Acoust. Soc. Am. 41 (1967) 138–147.
[34] G.S. Brown, The validity of shadowing corrections in rough surface scattering, Radio Sci. 16 (1984) 1461–1468.
[35] J.J. McCoy, Shadowing by randomly rough surfaces, J. Acoust. Soc. Am. 86 (1989) 1523–1529.
[36] M. Oren, S.K. Nayar, Generalization of Lambert's reflectance model computer graphics, Ann. Conf. Ser. (1994) 239–246.
[37] P.J. Lynch, R.J. Wagner, Rough-surface scattering: shadowing, multiple scatter, and energy conservation, J. Math. Phys. 11 (1970) 3032–3042.
[38] X.D. He, K.E. Torrance, F.X. Sillion, D.P. Greenberg, A comprehensive physical model for light reflection, Comp. Graph. 25 (1992) 175–186.
[39] C. Schlick, An inexpensive BRDF model for physically-based rendering, Eurographics 13 (1994) 233–246.
[40] D.A. Kapp, G.S. Brown, Effect of correlation between shadowing and shadowed points in rough surface scattering, IEEE Trans. Ant. Prop. 42 (1994) 1154–1160.
[41] S.O. Rice, The mathematical analysis of random noise, Bell Syst. Tech. J. 24 (1945) 46–156.
[42] T.K. Chan, Y. Kuga, A. Ishimaru, C.T.C. Le, Experimental studies of bistatic scattering from two-dimensional conducting random rough surfaces, IEEE Trans. Geo. Remote Sensing 34 (1996) 674–680.
[43] K.A. O'Donnell, E.R. Mendez, Experimental study of scattering from characterized random surfaces, J. Opt. Soc. Am. A 4 (1987) 1194–1205.
[44] J.N. Ford, K. Tang, R.O. Buckius, Fourier transform infrared system measurements of the bi-directional reflectivity of diffuse and grooved surfaces, J. Heat Transfer 117 (1995) 955–962.
[45] A.M. Smith, P.R. Muller, W. Frost, H.M. Hsia, Super- and subspecular maxima in the angular distribution of polarized radiation reflected from roughened dielectric surfaces, in: Progress Astronautics and Aeronautics: Heat Transfer and Spacecraft Thermal Control, J. Lucas, AIAA, New York, 1971, pp. 249–269.